



Shahrood University of
Technology



Iranian Society of
Mining Engineering
(IRSM)

Chemical Index of Alteration and its Relation to Mechanical Properties of Hydrothermally Uranium-Mineralized Rocks in Gabal Gattar Area, Northern Eastern Desert, Egypt

Yehia Z. Darwish¹, Abdelrahem Embaby ^{*2}, Samir M. Selim², Darwish M. El Kholy¹, Hani E. Sharafeldine², and Hussin A. Farag²

1. Nuclear Materials Authority of Egypt, P.O. Box 530, El Maadi, Cairo, Egypt

2. Mining and Petroleum Engineering Department, Faculty of Engineering, Al-Azhar University, Cairo, Egypt

Article Info

Received 16 May 2024

Received in Revised form 24 July 2024

Accepted 10 August 2024

Published online 10 August 2024

DOI: [10.22044/jme.2024.14535.2737](https://doi.org/10.22044/jme.2024.14535.2737)

Keywords

Chemical index of alteration

Mechanical properties

Hydrothermal alteration

Uranium mineralization

Gattar area

Abstract

The younger granites of Gabal Gattar area, Northern Eastern Desert of Egypt, host hydrothermal uranium mineralization at the northern segment of Gattar batholith and along its contacts with the oldest Hammamat sediments. The host rocks display many features of hydrothermal overprint results in changing their basic engineering characteristics as a function of variations of the degree of alteration. Progression from less altered to altered and mineralized rocks as the result of the alteration processes was assessed by the chemical index of alteration (CIA). The CIA numerical values were calculated by the molecular proportion of Al to the cations Ca, Na, and K. The studied rocks were divided into five grades according to degree of alteration and strength properties including: fresh (AG-I), slightly altered (AG-II), moderately altered (AG-III), highly altered (AG-IV) and very highly altered (AG-V). The strength properties of the studied rock units correlated well with the alteration grades assigned to them. That is, as the grade increased from AG-I to AG-V, abrasion resistance and crushability index increased, whereas compressive strength, slake durability and impact strength decreased.

1. Introduction

The basement complex of Gabal Gattar area is characterized by felsic-dominated magmatism that marks the culmination of the Pan-African igneous activity [1]. The intrusion of late Proterozoic younger granites in this region is accompanied by widespread hydrothermal activity indicated by the presence of hydrothermal ore deposits. The uranium mineralization in the northern parts of Gabal Gattar batholith is the most striking feature of this active hydrothermal activity, and has been extensively exploited for several decades by researchers from the Nuclear Materials Authority of Egypt. Previous studies which focused principally on the geology and structures of the ore bodies were described in details by many authors [2-7]. Contributions to mineralogy and geochemistry revealed that the host granite is

perthitic alkali feldspar granite and the main uranium minerals are uranophane and kasolite with minor abundance of pitchblende [4, 7-9]. Remote sensing and geophysical studies were investigated by [10-12]. Other few studies which have dealt with the physical and mechanical properties of the exposed rocks in Gabal Gattar area have been carried out by Haridy [13] and Salah El-Din [14]. Haridy studied the relation between the physical and mechanical properties and the spatial distribution of the joint-type uranium mineralization in Gattar area. He statistically treated the field measurements of the structural elements affecting both the granite and the Hammamat sedimentary rocks and delineated the paleostress affecting the area. He also determined the chronological sequence of these

✉ Corresponding author: Abdel-raheemkhalifa.12@azhar.edu.eg (A. Embaby)

paleostress and then described the structural evolution of Gabal Gattar area. Salah El-Din discussed the effect of the geotechnical properties of Gattar granites on underground mining and estimated the rock mass quality and support elements for study area.

The uranium mineralization of Gabal Gattar area is classified as granite-related hydrothermal uranium deposits, which is subdivided into intragranitic and perigranitic subtypes. Uranium was mined out from two main localities: Gattar-II (G-II) and Gattar-V (G-V) uranium occurrences. The exposed rock types at the two occurrences show clear evidence of hydrothermal activity throughout the mineralized zones. The intensive hydrothermal alteration and the recent surficial weathering cause many changes in the principle mineralogical and chemical compositions of the host rocks. These variations are intern affecting the engineering properties of the rock as a result of formation of new mineral phases.

Weathering indices calculated based on whole-rock chemical analyses are widely used for evaluating the intensity of alteration [15-17]. Recent researches have demonstrated that weathering indices based on the ratio of a set of mobile oxides to one or more immobile oxides are valuable criteria for describing changes caused by weathering and hydrothermal alteration [18-20]. These indices can be used to indirectly characterize the engineering properties of the altered rocks, specially the weathered granite [21].

Our work summarizes the field observations, geochemical data and the results of the mechanical tests of the unaltered and altered mineralized rocks from Gabal Gattar area. The main objectives of this study were to measure the degree of alteration and assess its link with the mechanical properties throughout the unaltered and altered rocks. A proposed classification scheme of alteration grades is used in this study to designate various rock groups in terms of degree of alteration and mechanical properties.

2. Geological Overview of Gabal Gattar Area

2.1. Regional geological setting

The late Proterozoic basement complex of Gabal Gattar area is located in the northern Eastern Desert of Egypt (Figure 1a), 40km west of Hurghada city (latitudes 26°51'25"N 27°08'52"N and longitudes 33°13'00"E, 33°25'59"E). The main rock type is the younger granitic rocks of Gabal Gattar (605Ma) [22]. It is surrounded by older rocks consisting of metavolcanics, older

granites and Hammamat sediments of molasse type (Figure 1b).

The Gattar granitic batholith shows sharp intrusive contacts against these rocks. The metavolcanics are exposed in the center of the batholith as roof pendants over the Gattar granites at Gabal Kehla. They are predominating by metabasalts and metadolerites [4]. The older granites surrounded the batholith as low to moderated outcrops and contain diorite, quartz diorite and granodiorite [23]. The Hammamat sediments are covering the northern parts of Gabal Gattar area. They are forming the southern extension of Gabal Um Tawat. These rocks comprise greenish and brownish siltstone and greywack interbedded with minor conglomerate [24].

The northern segment of Gabal Gattar area contains many uranium showings of lensoid ore bodies grouped into seven uranium occurrences (Gattar-I to Gattar-VII), extending over some few kilometers along the northern faults. The uranium ore bodies are hosted by Gabal Gattar granite at its northern peripheries. There, the oldest Hammamat sediments show sharp contact with this granite and host a perigranitic uranium occurrence (Gattar-V occurrence). The other uranium localities are located in the granite. The most significant uranium ore bodies in Gattar area occur in G-II and G-V uranium occurrences, which were selected in this study (Figure 1b).

2.2. G-II Uranium Occurrence

G-II uranium occurrence is a triangular granitic mass invaded by numerous quartz veins and basic dikes of doleritic composition. The granite forms high rough mountain with sharp rugged peak (Figure 2a). It is highly sheared, jointed, fractured and altered in many parts. This granite is medium- to coarse-grained perthitic alkali feldspar granite; range in color from pink or slightly red to dark or reddish brown which depends mainly on the type of wall-rock alterations. It is mainly composed of potash feldspar (perthite) and quartz with subordinate amount of plagioclase. Accessory minerals comprise biotite, muscovite, zircon, monazite, fluorite, apatite and iron oxides. Chlorite, muscovite kaolinite, sericite and epidote, which could be considered as secondary minerals, also appear in the unaltered samples.

Excavation includes tunnels, surface trenches and open pit, which distributed along the eastern and western sides of this granitic mass. The fresh

granite shows different wall-rock alterations as the result of the impact of hydrothermal solutions. The hydrothermal alterations consist of multiple overprinted phases. This is evident as silicification, hematization, kaolinization,

fluoritization and chloritization as well as manganese oxides (Figure 2b-e). Uranophane is the principle uranium mineral but pitchblende also occurs in minor amount.

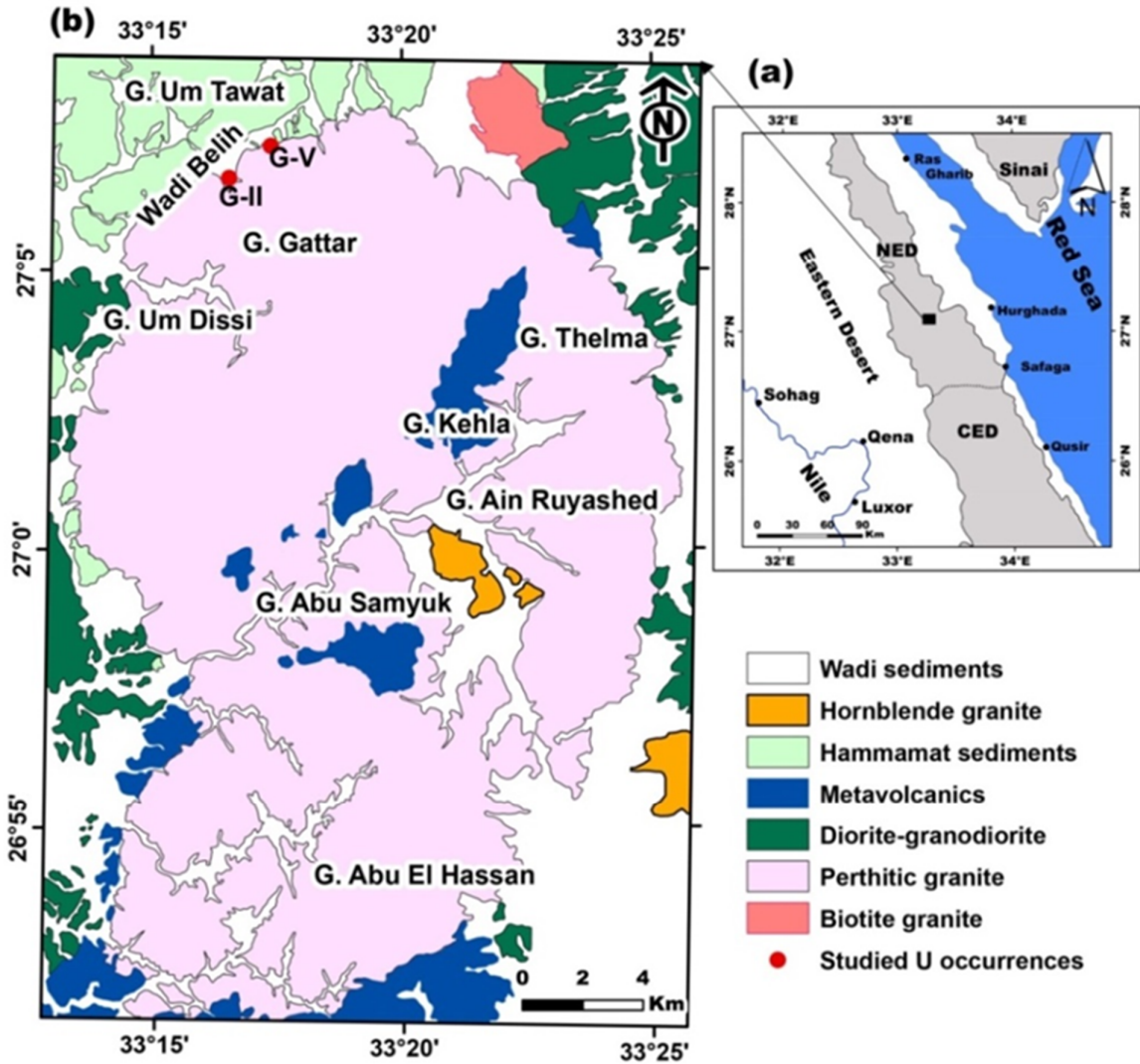


Figure 1. (a) Location of the study area in the northern Eastern Desert of Egypt. (b) Geological map showing the different rock types exposed at Gabal Gattar area and illustrating the locations of the studied uranium occurrences (modified after [4])

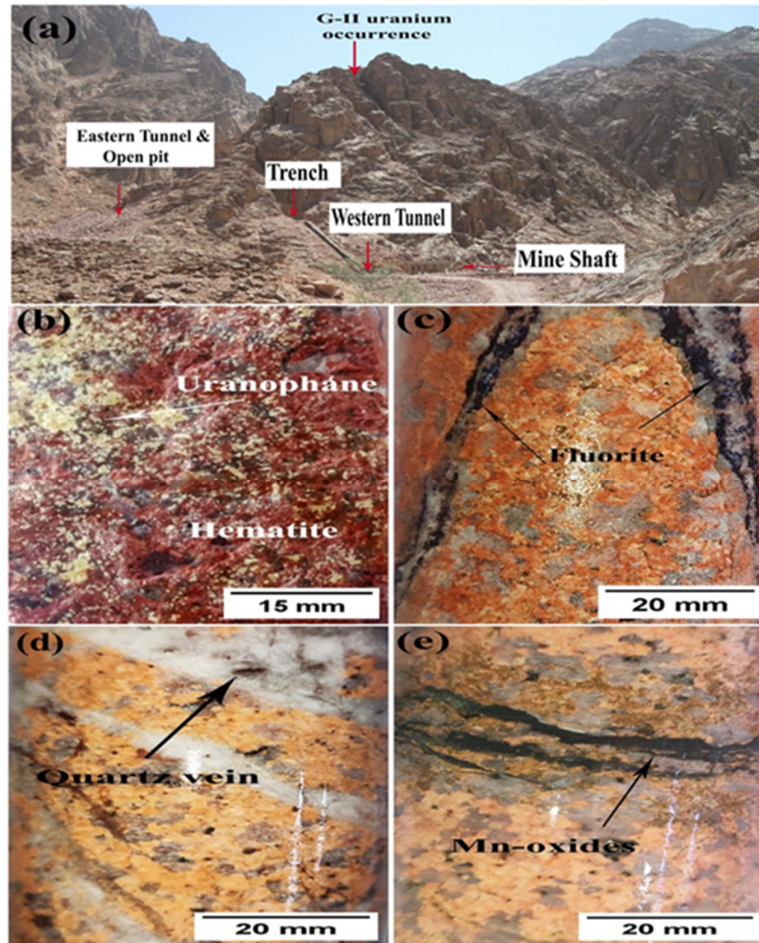


Figure 2. Field photograph showing. (a) The granitic massif of G-II uranium occurrence forms high rough mountain with sharp rugged peak, looking south. (b) Uranophane is the principle uranium mineral in G-II uranium occurrence and usually associated with hematitization. (c) Fracture-filling fluorite in the altered granite. (d) Veinlets of quartz (silicification). (e) Manganese oxides filling the microfractures of the granite.

2.3. G-V Uranium Occurrence

The exposed rocks in G-V are the Hammamat sediments and the perthitic granite of Gabal Gattar. The unaltered Hammamat essentially consists of sand-size, angular to subangular grains of quartz and feldspars, together with subordinate lithic fragments, set in a fine recrystalline matrix of the same constituents in addition to chlorite and iron oxides. Carbonates (mainly calcite) are not only found as crack fillings, but also as patches within the matrix.

The important mineralized zone at G-V area is located in the middle portion of the mapped area, along the contact between the Hammamat sediments and the Gattar granite (Figure 3a). This mineralized zone is excavated by exploratory tunnel and small trenches. The contact zone between Hammamat sediments and Gattar granite is associated with widespread post-magmatic hydrothermal alterations accompanied the precipitation of secondary uranium mineralization. These secondary minerals are often with brighter yellow color, and consist mainly of uranophane and kasolite (Figure 3b).

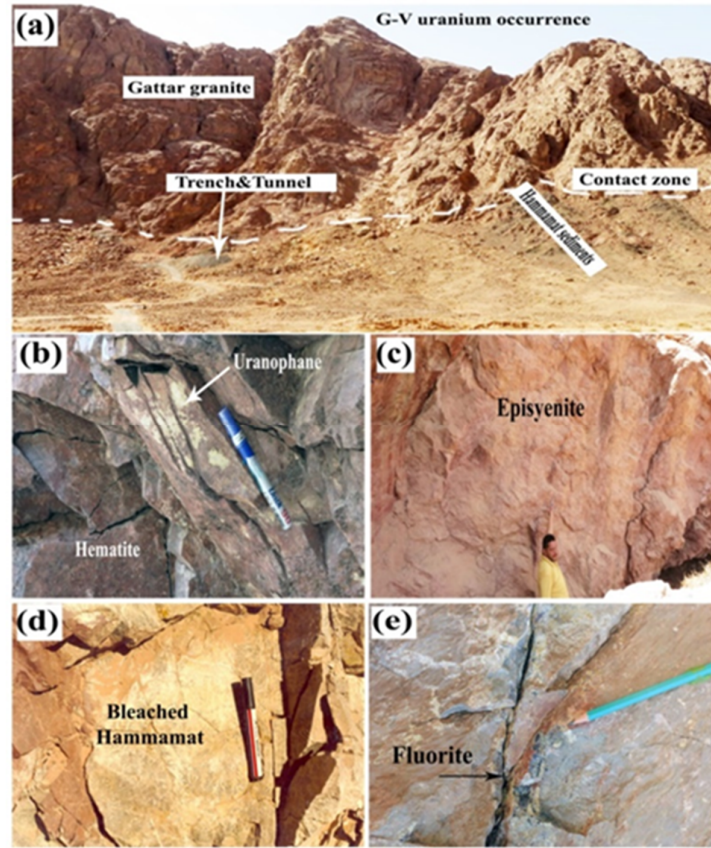


Figure 3. Field photographs showing. (a) G-V uranium occurrence is located along the contact between Hammamat sediments and Gabal Gattar granite. (b) Uranophane staining the joint surfaces of the hematitized Hammamat variety. (c) Episyenite displaying different colors due to alteration of the granite. (d) Bleached Hammamat variety with creamy color as a result of alteration of the original Hammamat. (e) Dark purple fluorite in the hematitized Hammamat.

The uranium mineralization is limited to the Hammamat, with little mineralization in the nearby altered granite. The common alteration features associated with the Hammamat sediments are the bleaching (Figure 3c) strong hematitization, fluoritization (Figure 3d) besides carbonatization, kaolinitization and some manganese dendrites.

The main wall-rock alteration feature manifested in the Gattar granite of G-V occurrence is the episyenitization of the granite (disilicification). The episyenitization process almost occurs near the margins of the granitic pluton, which is closely associated with tectonic tensional fracturing. The irregular episyenitized bodies of the Gattar granite are of indefinite margins that grade into unaltered granite. They are porous, displaying different colors of light pink, reddish to reddish brown and dark brown (Figure 3e). Generally, gradation from weakly-moderately- to strongly episyenitization can be

noticed according to the range of dissolution of the magmatic quartz.

3. Materials and methods

3.1. Sample collection and description

To achieve the requirements of the present study, block sizes of 23 rock samples have been collected from G-II and G-V uranium occurrences. The studied samples were generally collected from outcrops, tunnels, open pits and trenches, which previously excavated in both two occurrences. The altered samples were mainly chosen from the mineralized zones where the wall-rock alteration is more intense and the uranium mineralization is distinct. The unaltered varieties were chosen from areas with minimum alteration features as possible. Locations of the collected samples from the studied occurrences are shown in Figs (4 and 5). Moreover, hand sample description for each rock material was determined and listed in Table (1).

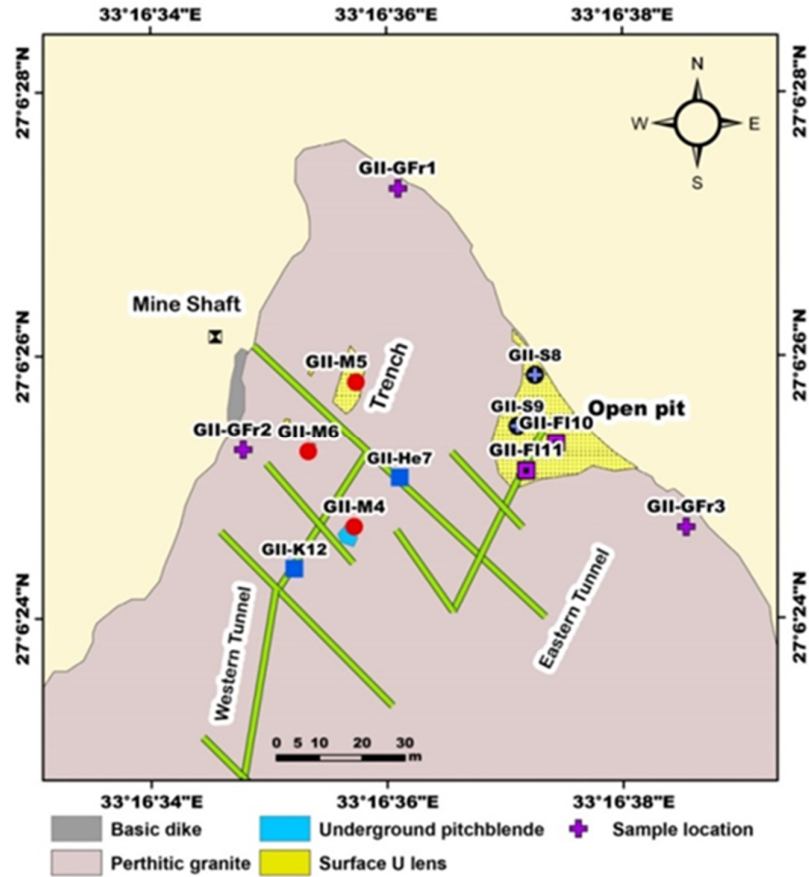


Figure 4. Locations of the studied samples in G-II uranium occurrence.

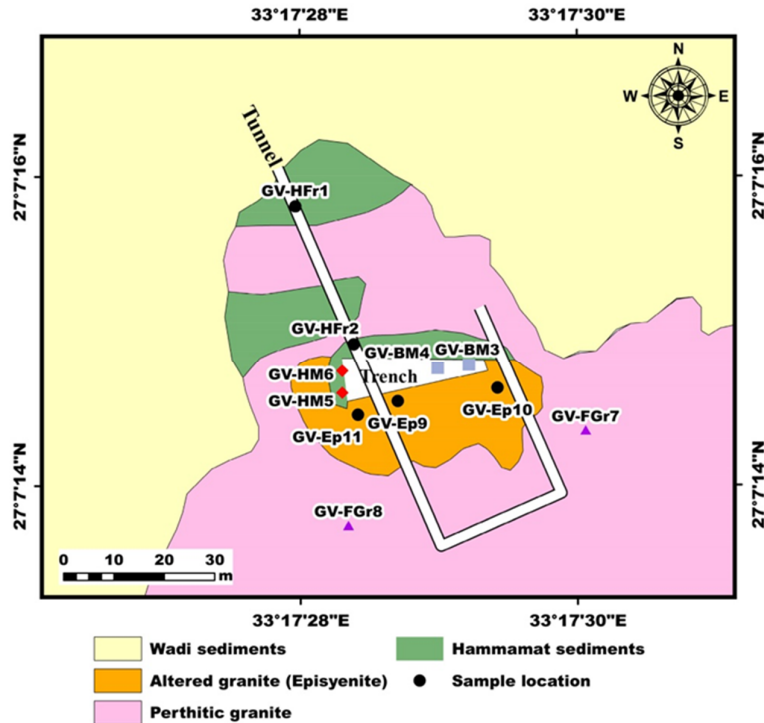


Figure 5. Locations of the collected samples in G-V uranium occurrence.

3.2. Laboratory Chemical Analyses

For chemical analyses, the samples were ground and sieved through a 74 μm sieve size. They were then dried in an oven for a whole night at 105 ± 5 °C to ensure total dryness. To determine the loss on ignition (L.O.I.%) for each prepared sample, a portion of the sample was ignited at 1000 °C following the standard test procedure ASTM E-1621 [25]. The chemical analyses for the major components were determined according to Shapiro and Brannock procedure [26]. With a relative accuracy of 1%. SiO_2 , Al_2O_3 , TiO_2 and P_2O_5 contents were analyzed using relevant spectrophotometric methods while Na_2O and K_2O concentrations were determined by the flame photometric technique. Titration methods were used to analyze Fe as Fe_2O_3 , MgO , and CaO . On the other hand, spectrophotometric analyses of U and Th were performed using a chromogenic reagent

Arsenazo-III [27] with a relative accuracy of 5%. All the chemical laboratory analyses were carried out in the Nuclear Materials Authority of Egypt.

3.3. Engineering Tests

The mechanical properties of the studied samples were evaluated using the following tests: uniaxial compressive strength (UCS), slake durability index (SDI), Los Angeles abrasion (LAA), crushability index (CI) and impact strength index (ISI).

3.3.1. Uniaxial Compressive Strength Test (UCS)

Sample preparation for UCS involved rock machining for cutting to sizes using a rock cutting machine into prismatic samples with dimensions of 10 x 10 x 20 cm (Figure 6a-d), equivalent to a height and width ratio of 2 : 1.

Table 1. Hand specimen description of the collected unaltered and altered uranium-mineralized samples from G-II and G-V uranium occurrences.

Sample No.	Degree and type of alteration	Description of hand specimen
GII-FG1	Fresh granite	Buff, medium-grained alkali feldspar granite stained with slight kaolinitization
GII-FG2	Fresh granite	Light pinkish, medium- to coarse-grained alkali feldspar granite, the microfractures are filled with quartz that causing slight silicification
GII-FG3	Fresh granite	Whitish buff, medium-grained alkali feldspar granite stained with slight manganese dendrites
GII-M4	Altered mineralized granite	Buff to reddish brown, medium to coarse-grained, highly sheared and brecciated alkali feldspar granite contains dark patches of pitchblende
GII-M5	Altered mineralized granite	Highly hematitized and kaolinitized, whitish to reddish buff medium-grained alkali feldspar granite stained with secondary yellow U minerals
GII-M6	Altered mineralized granite	Dark brown highly hematitized, medium-grained alkali feldspar granite stained with secondary yellow U minerals
GII-He7	Hematitized non-mineralized granite	Reddish brown highly hematitized medium-grained alkali feldspar granite, biotite is chloritized
GII-S8	Silicified non-mineralized granite	Light pink, highly silicified, medium to coarse-grained alkali feldspar granite, secondary quartz grains are filling the interstitial spaces between minerals
GII-S9	Silicified non-mineralized granite	Highly silicified and hematitized medium- to coarse-grained alkali feldspar granite, quartz is filling fractures of the sample
GII-F10	Fluoritized mineralized granite	Light pink, medium- to coarse-grained alkali feldspar granite stained with secondary yellow U minerals and contains veinlets of purple to dark purple fluorite
GII-F11	Fluoritized mineralized granite	Silicified, medium- to coarse-grained alkali feldspar granite stained by hematite and secondary yellow U minerals, the microfractures are filled by fluorite
GII-K12	Kaolinitized non-mineralized granite	Whitish light pink, kaolinitized medium-grained alkali feldspar granite stained by manganese dendrites
GV-HFr1	Fresh greywacke	Greenish grey, highly sheared medium-grained Hammamat greywacke
GV-HFr2	Fresh siltstone	Dark grey, highly sheared fine-grained Hammamat siltstone
GV-BM3	Bleached mineralized siltstone	Bleached fine-grained Hammamat siltstone with creamy color stained with secondary yellow U minerals and Mn-oxides
GV-BM4	Bleached non-mineralized siltstone	Bleached fine-grained Hammamat siltstone with creamy color stained with Mn-oxides
GV-HM5	Hematitized mineralized siltstone	Hematitized, reddish grey fine-grained siltstone, stained with secondary yellow U minerals and contains veinlets of fluorite
GV-HM6	Hematitized mineralized siltstone	Hematitized and carbonatized reddish to whitish grey fine-grained siltstone stained with secondary yellow U minerals
GV-FG7	Fresh granite	Buff medium- grained alkali feldspar granite, biotite is chloritized
GV-FG8	Fresh granite	Whitish buff medium- grained alkali feldspar granite, biotite is chloritized and feldspars are slightly kaolinitized
GV-Ep9	Episyenitized granite	Porous, reddish brown hematitized episyenitized granite
GV-Ep10	Episyenitized granite	Porous, whitish light pink kaolinitized episyenitized granite
GV-Ep11	Episyenitized granite	Porous, reddish brown hematitized and kaolinitized episyenitized granite

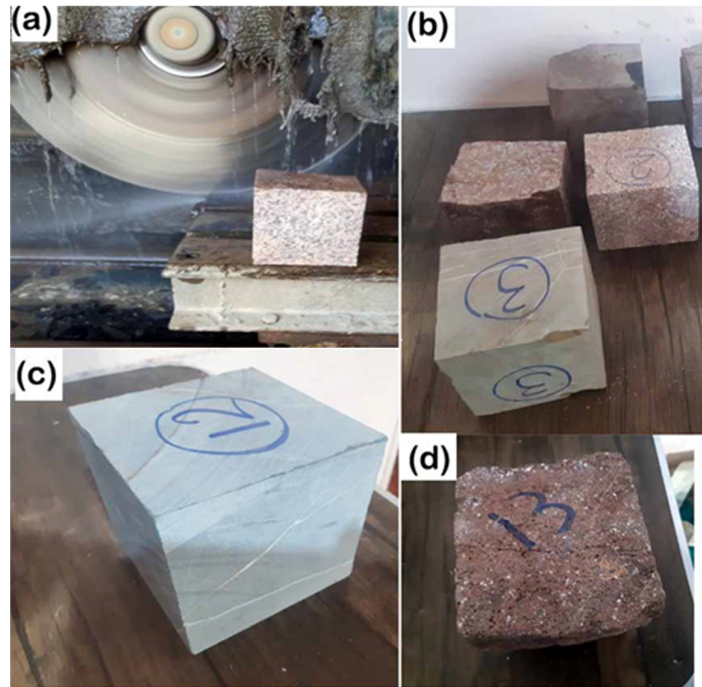


Figure 6. (a) The used rock cutting machine in this study. (b), (c) and (d) Prismatic rock samples with dimensions 10 x 10 x 20cm.

The aim of this test is to determine the unconfined (or uniaxial) compressive strength of rock specimens. The procedure for the test is as stated in ISRM [28]. It was carried out in The General Authority for Execution of mining and Industrial Projects, Central laboratories, Helwan, Egypt. A computerized compression machine was used to conduct the uniaxial compression test. The electronic gauge, piston, and two spherical seated platens that make up the uniaxial testing machine are employed to lessen the impact of the specimen's non-parallelism on the test results as the lower loading plate moves upward. Accurate centering is required for the specimen, platen, and spherical seat with regard to both the loading device and each other. This will guarantee that the load is spread equally over the specimen. The Volumetric strain is calculated from the ratio of Axial strain to lateral strain as follows:

$$r_c = \frac{\rho_{max}}{A} \quad (\text{MPa})$$

Where r_c is the uniaxial compressive strength (UCS) of the rock (MPa), ρ_{max} is the peak load (kN) and A is the initial cross sectional area of specimen (m^2).

3.3.2. Los Angeles Abrasion (LAA)

The abrasion resistance tests were conducted on the collected samples in accordance with

ASTM C131/131M [29], using a LAA test apparatus in the General Authority for Execution of mining and Industrial Projects, central laboratories, Helwan, Egypt. The LAA test is based on calculating the percentage of wear which is brought by the relative rubbing action between steel balls and the aggregates. Some scientists think that this test is more reliable, because the rubbing and hammering motion simulate the field conditions where both abrasion and impact occur. The LAA test apparatus is comprised of a hollow steel drum measuring 711 mm in inner diameter, including an inside shelf that is 25 mm thick and 90 mm deep. According to ASTM C 131–131M [29] standard, one set of samples for each kind of rock was prepared to aggregate sizes with a graded mix of 37.5–25 mm, 25–19 mm, 19–12.5 mm, and 12.5–9.5mm size fractions. This grade of the test samples was prepared by crushing the samples by hammers. After that, each test sample (around 5000g) was put in a steel drum with 12 or 11 steel spheres. The hatch cover was fastened in position, and the drum was turned 500 times at a speed of 30 to 33 revolutions per minute. Crushed aggregate particles and the steel spheres (charge) were poured onto a tray set after 500 rotations were finished. The crushed aggregate particles were sieved through 1.7mm. The aggregate coarser than the 1.70 mm was oven-dried for 24 hours at 110°C to a constant mass. The LAA was expressed in percentage as follow:

$$\text{LAA (\%)} = \frac{\text{Original weight} - \text{weight retained on 1.7mm}}{\text{Original weight}}$$

3.3.3. Slake Durability Index (SDI)

The main objective of this test is to evaluate the resistance of a sample to weakening and disintegrating under cycles of drying and wetting. The test procedure is in accordance with ASTM D4644 [30] standard practice. The standard is based on two cycles of drying and wetting. For assessing rocks with greater durability, four or five cycles of drying and wetting are recommended. A sample including ten rock fragments, each weighing between 40 and 60 g, was chosen for each SDI test. The total weight of the sample ranges from 450 to 550 g. The sample was put within a screen drum, and both were oven-dried to a consistent weight at $110^{\circ} \pm 5^{\circ} \text{C}$. After the sample had cooled to room temperature, the drum was connected to a motor and rotated with a speed of 20 rpm while submerged in distilled water for 10 minutes. The sample was oven-dried at $110^{\circ} \pm 5^{\circ} \text{C}$ for a constant weight. After that the sample was subjected to a second wet and dry cycle. The SDI is defined "as percentage ratio of final and initial dry mass of rocks" in the drum. The SDI is calculated using this formula:

$$\text{SDI} = \frac{W_n - C}{W_i - C} \times 100$$

Where W_n and W_i are mass of drum plus oven-dried specimen before the n and first slake durability index testing cycle, C is mass of drum, and n is a number of cycles of slake durability index test.

3.3.4. Crushability index (CI)

The CI test requires a laboratory jaw crusher that can be used in crushing experiments. The samples selected from the field were crushed using a hand hammer to obtain small sizes that are suitable for the crusher feed opening. Range of feeding size is 12–20mm. After the crushing process, the sieving is performed to obtain 500 grams of the selected size range for each sample. The samples are dried in the electric oven for 48 hours at a temperature of 110°C . The outlet gap of the jaw plates were adjusted to 8-12 mm. A sieve with 9.5 mm size was used to filter crushed materials, and the proportion of undersized material was reported as the crushability index (CI). For every type of rock, the test was

conducted two or three times, and the average results were noted as the CI.

3.3.5. Impact strength test (ISI)

In the impact strength testing, a device designated by Evans and Pomeroy [31], was employed. A crushed sample in the size range 3.18-9.52mm was oven dried for 48 hours at 110°C . A hammer with 1.8 kg weight was dropped 20 times from a height of 30.48 cm upon a 100g crushed sample that was placed in 42.86 mm diameter cylinder. The quantity of sample that retained in the original size range is equal to the ISI value. For every rock type, the test was conducted three times, and the average value was noted as the ISI.

4. Results and Discussion

4.1. Major oxides characteristics

Major oxides (wt.%) compositions as well as U and Th concentrations (ppm) of 23 samples of the studied rocks from G-II and G-V uranium occurrences are compiled in Tables (2 and 3). Five rock varieties were discriminated in the studied occurrences, which represent the unaltered and altered uranium-mineralized rocks including (1) unaltered Gattar granite, (2) altered and mineralized Gattar granite, (3) unaltered Hammamat, (4) altered and mineralized Hammamat (bleached and hematized), and (5) episyenitized granite. The oxide contents of altered rocks provide information about the degree of alteration and could be related to the differences in mineralogical and chemical compositions.

Unaltered Gabal Gattar granite was classified as alkali feldspar granite [4]. The analyzed granitic samples have relatively high SiO_2 contents (74.41-76.42 wt. %). In addition to the high silica content, Na_2O (3.88-4.18 wt. %) and K_2O (3.98-4.51wt.%) are fairly high. Whereas the other major oxides, TiO_2 (0.08-0.12 wt. %), Fe_2O_3 (1.16-1.62 wt. %), MgO (0.12-0.22 wt. %), CaO (0.25-0.58 wt. %) and P_2O_5 (0.02-0.05wt.%) are relatively low (Tables 2 and 3). The analyzed unaltered Hammamat sediments are characterized by a wide variation in their composition with SiO_2 (62.21-66.19 wt. %), TiO_2 (0.65-0.76 wt.%), Al_2O_3 (14.93-16.65 wt.%), Fe_2O_3 (2.86-3.42 wt.%), MgO (1.97-2.07 wt.%), Na_2O (2.68-3.19 wt.%) and K_2O (1.66-2.18 wt.%; Table 3). The geochemical data of the greywacke and siltstone show that they are characterized by $\text{Na}_2\text{O}/\text{K}_2\text{O} > 1$ and $\text{Al}_2\text{O}_3/\text{Na}_2\text{O} = 5.2-5.6$ (Table 6.2).

The altered and mineralized granite is characterized by enrichment of SiO_2 (70.18-78.13 wt. %), especially in the silicified samples. Al_2O_3 (12.51-15.2 wt. %) is enriched along the altered samples. The hematitized samples show enrichment of Fe_2O_3 (0.98-5.23 wt. %). TiO_2 (0.08-1.06 wt. %), MgO (0.18-0.45 wt. %) and CaO (0.34-1.43 wt.%) also display high values compared to the unaltered precursor. On the other hand, Na_2O (3.36-3.88 wt. %) and K_2O (2.75-4.36 wt. %) show slight depletion relative to the unaltered granite (Table 2).

One of the most prominent features in the episyenitized granite is the depletion of SiO_2 contents (61.14-67.32 wt. %). Al_2O_3 (20.16-21.65 wt. %) is enriched and TiO_2 (0.11-0.16 wt. %) is relatively constant relative the unaltered granite (Table 3). The high aluminum contents are the result of development of kaolinite-rich clays, which are the main factor for reducing the strength properties of the altered rocks. A true addition of total iron is noticed in the episyenitized granite. The oxidation of Fe is evident by the decrease of FeO (0.33-0.41 wt. %) and an accompanying increase of Fe_2O_3 (2.41-10.13 wt. %). MgO (0.33-0.45 wt. %) exhibits marked enrichment and CaO (0.18-0.45 wt. %) shows high depleted values.

In the altered mineralized siltstone, SiO_2 contents are generally constant (63.25-66.78 wt. %) compared to the unaltered equivalent. The values of Al_2O_3 (14.61-18.31wt. %) and TiO_2 (0.55-0.85wt. %), do not show large differences relative to the unaltered siltstone (Table 3). Fe_2O_3 is highly enriched in the hematitized samples, began to decrease in the bleached mineralized samples where the sericite increases and the iron is removed. CaO (0.66-0.97 wt. %) and MgO contents (0.77-1.22 wt. %) are decreased, while K_2O (3.31-4.21 wt. %) shows extreme enrichment due to the development of secondary sericite.

4.2. Evaluation of the degree of alteration

The chemical index of alteration (CIA) has been applied to our samples to assess the degree of alteration. It was calculated according to Nesbitt and Young formula [32]. For each sample as shown in Tables (2 and 3), the increase of CIA values can be attributed to the loss of mobile cations and alteration of the crystal structure [33].

Index values do not exhibit large changes among the unaltered samples. In particular, CIA values in unaltered granite and Hammamat samples range from 49.9 to 52.6 and from 53.3 to 54.1, respectively (Tables 2 and 3). Mobile oxides (CaO , Na_2O and K_2O) are highly removed from the rock at final stages of alteration. As a result, drastic changes in the common patterns of chemical index are observed (Figure 7). The fact that a majority of unaltered samples are above a CIA of 50 suggests that significant aqueous alteration took place. The mineralized granitic samples from G-II occurrence have CIA values with an average of 55.2, slightly higher than the unaltered equivalent.

The CIA values are increased towards the mineralized Hammamat sediments (av. 71.1) in G-V occurrence. The Episyenitized samples report the highest group of CIA values with an average of 78.2. Overall, CIA values are increasing, going up from unaltered to mineralized rocks, and are above 70 for a large majority of mineralized samples from G-V occurrence.

The geochemical analyses of the studied rock units indicated that major oxide values are changed in the transition from fresh rock to altered rock in each rock type from Gabal Gattar area. Changes of major oxides with CIA are illustrated in Figure 8. It is indicated that almost all the major oxides were mobilized during alteration and mineralization. Even typically immobile elements such as Ti and Al display significantly mobile behaviors during hydrothermal processes. Overall the studied rocks, strong negative relationship between SiO_2 and CIA is directly related to the dissolution of magmatic quartz. Al_2O_3 is positively correlated with CIA, because of development of kaolinite-rich clay minerals among the last degrees of alteration. A moderate positive correlation is observed between Fe_2O_3 and CIA due to the close spatial association of hematitization and uranium mineralization. Na_2O is decreased sharply with increasing CIA, which reflects high alteration rate of Ca-plagioclase in the granite. In all series, the contents of TiO_2 remain constant along the fifth degrees of alteration, while MgO , Ca and K_2O show scattering with weak correlations.

Table 2. Major oxides (wt.%), U and Th (ppm) contents of the granitic rocks from G-II uranium occurrence.

Rock type	Unaltered Gattar granite						Altered and uranium- mineralized Gattar granite					
Sample No.	GII-FG1	GII-FG2	GII-FG3	GII-M4	GII-M5	GII-M6	GII-He7	GII-S8	GII-S9	GII-F10	GII-F11	GII-K12
Major oxides (wt.%)												
SiO ₂	76.24	75.95	76.42	70.18	71.29	71.6	72.15	78.13	76.1	74.12	72.23	73.66
TiO ₂	0.08	0.1	0.08	0.09	1.03	0.08	0.09	0.08	0.1	1.02	1.06	0.08
Al ₂ O ₃	12.53	11.98	12.1	14.62	13.35	14.18	13.33	12.55	12.51	13.86	14.44	15.2
Fe ₂ O ₃	1.22	1.45	1.16	3.29	3.12	4.6	5.23	1.26	2.16	1.35	1.68	0.98
FeO	0.19	0.62	0.32	1.12	1.18	1.25	0.41	0.24	0.36	0.22	0.42	0.11
MnO	0.01	0.02	0.02	0.38	0.21	0.08	0.09	0.05	0.08	0.04	0.06	0.09
MgO	0.18	0.22	0.12	0.45	0.37	0.29	0.25	0.23	0.27	0.22	0.18	0.26
CaO	0.25	0.58	0.32	0.65	0.52	0.38	0.42	0.36	0.34	1.23	1.43	0.35
Na ₂ O	4.12	3.95	4.18	3.75	3.88	3.36	3.77	3.82	3.75	3.66	3.85	3.49
K ₂ O	4.51	3.98	4.42	4.1	3.92	3.68	3.65	2.75	3.62	3.61	4.08	4.36
P ₂ O ₅	0.02	0.03	0.03	0.06	0.04	0.02	0.05	0.02	0.03	0.05	0.04	0.05
L.O.I	0.56	1.08	0.81	1.23	0.86	0.45	0.54	0.48	0.63	0.56	0.51	1.31
Total %	99.91	99.96	99.98	99.92	99.77	99.97	99.98	99.97	99.95	99.94	99.98	99.94
CIA	50.9	50.4	49.9	55.7	53.8	58.3	55.2	56.0	54.1	53.5	52.1	58.1
Radioelement concentrations (ppm)												
U	15.4	8.6	11.9	3855	2941	3161	264	45.8	32.9	1834	2764	28.4
Th	21.9	14.3	24.3	37.1	33.5	39.2	41.8	58.6	29.6	31.8	41.2	25.4
Th/U	1.42	1.66	2.04	0.01	0.01	0.01	0.16	1.28	0.90	0.02	0.01	0.89

Table 3. Major oxides (wt.%), U and Th (ppm) concentrations of the unaltered and altered uranium-mineralized rocks from G-V uranium occurrence.

Rock type	Unaltered Hammamat		Bleached mineralized Hammamat		Hematitized mineralized Hammamat		Unaltered Gattar granite		Episytenitized granite		
Sample No.	GV-HFr1	GV-HFr2	GV-BM3	GV-BM4	GV-HM5	GV-HM6	GV-FG7	GV-FG8	GV-Ep9	GV-Ep10	GV-Ep11
Major oxides (wt.%)											
SiO ₂	62.21	66.19	66.78	66.59	64.67	63.25	74.41	75.27	61.14	67.32	66.93
TiO ₂	0.76	0.65	0.85	0.62	0.55	0.67	0.12	0.08	0.13	0.11	0.16
Al ₂ O ₃	16.65	14.93	18.31	17.55	14.91	14.61	13.27	12.76	20.16	21.65	20.22
Fe ₂ O ₃	3.42	2.86	1.84	2.48	8.76	10.45	1.62	1.45	10.13	2.41	5.12
FeO	1.27	0.75	0.18	0.15	0.36	0.31	0.55	0.36	0.33	0.41	0.37
MnO	0.18	0.12	0.04	0.04	0.06	0.07	0.06	0.04	0.12	0.09	0.1
MgO	2.07	1.97	0.87	0.77	1.1	1.22	0.22	0.17	0.45	0.33	0.37
CaO	4.54	3.38	0.74	0.66	0.92	0.97	0.56	0.47	0.45	0.18	0.36
Na ₂ O	2.68	3.19	0.82	0.71	0.97	0.95	3.88	4.13	1.28	1.17	1.63
K ₂ O	2.18	1.66	4.21	4.04	3.31	3.61	4.31	4.19	2.88	3.16	2.54
P ₂ O ₅	0.17	0.21	0.18	0.14	0.17	0.22	0.05	0.05	0.09	0.05	0.06
L.O.I	3.79	3.62	5.12	6.23	4.17	3.61	0.91	1.02	2.55	3.1	2.13
Total %	99.92	99.53	99.94	99.98	99.95	99.94	99.96	99.99	99.71	99.98	99.99
CIA	53.3	54.1	72.9	73.3	69.8	68.5	52.6	51.4	77.6	79.6	77.3
Radioelement concentrations (ppm)											
U	6.8	5.2	4731	3589	5277	11248	8.9	10.5	55.2	31.8	18.4
Th	3.8	4.2	10.2	5.2	8.4	12.8	18.4	19.7	16.4	25.1	29.7
Th/U	0.56	0.81	0.002	0.001	0.002	0.001	2.06	1.87	0.29	0.78	1.61

CIA: Chemical Index of Alteration [32], calculated in molar proportion as $[\text{Al}_2\text{O}_3/(\text{Al}_2\text{O}_3+\text{CaO}+\text{Na}_2\text{O}+\text{K}_2\text{O})]100$.

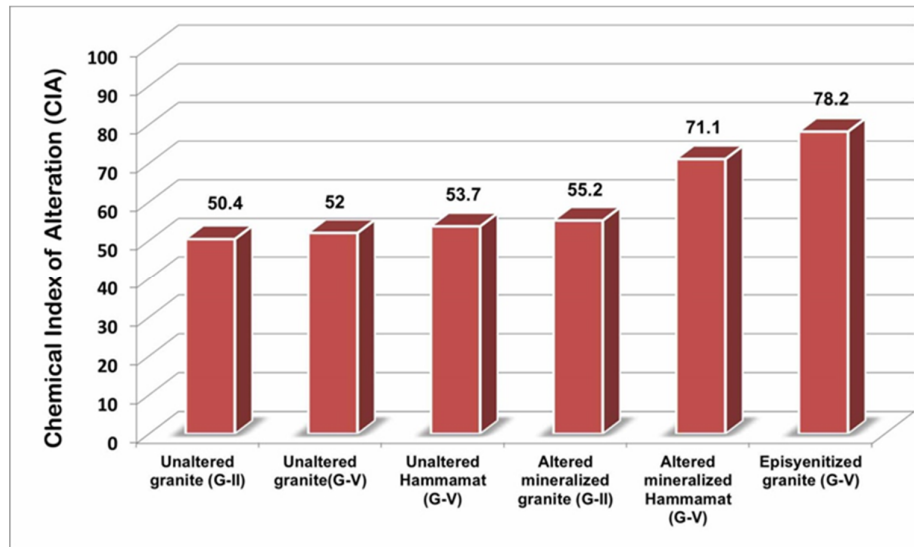


Figure 7. Histogram showing the average CIA values for the studied rock types from G-II and G-V uranium occurrences.

4.3. U and Th Distribution

The unaltered Gattar granite has high background values of U and Th. The U contents range from 8.6ppm to 15.4ppm, whereas Th contents are varying between 14.3ppm and 24.3ppm. Th/U ratios (1.42 to 2.07) are relatively lower than the normal value for the acidic igneous rocks ($Th/U=3$) [34], Tables 2 and 3). The U contents of the unaltered Hammamat sediments (5.2-6.8ppm) are higher than that of average greywacke (1.5ppm) [35]. Thorium contents (3.8-4.2ppm) are getting near the average of greywacke (5ppm), [35].

U is enriched in the altered varieties range from 28.4-3855ppm, 18.4-55.2ppm and 3589-11248ppm for the mineralized granite, episyenitized granite and mineralized Hammamat,

respectively. Uranium enrichment is associated with a relatively weak increase in Th contents along the mineralized rocks. Th/U ratios are generally decreased with extremely lower values noticed in the mineralized Hammamat (Table 3). The relations between U and Th with CIA are graphically presented in Figure 9. It was shown that U amounts are increased along the first four grades (AG-1 to AG-4) and began to decrease in grade AG-V. It is indicated that with progressive alteration, U is leached out from the rock under the effect of the multiphase of the hydrothermal solutions. The weak positive correlation between Th and CIA can be attributed to irregular distribution of Th along the altered stages and relative immobility of Th in the hydrothermal conditions.

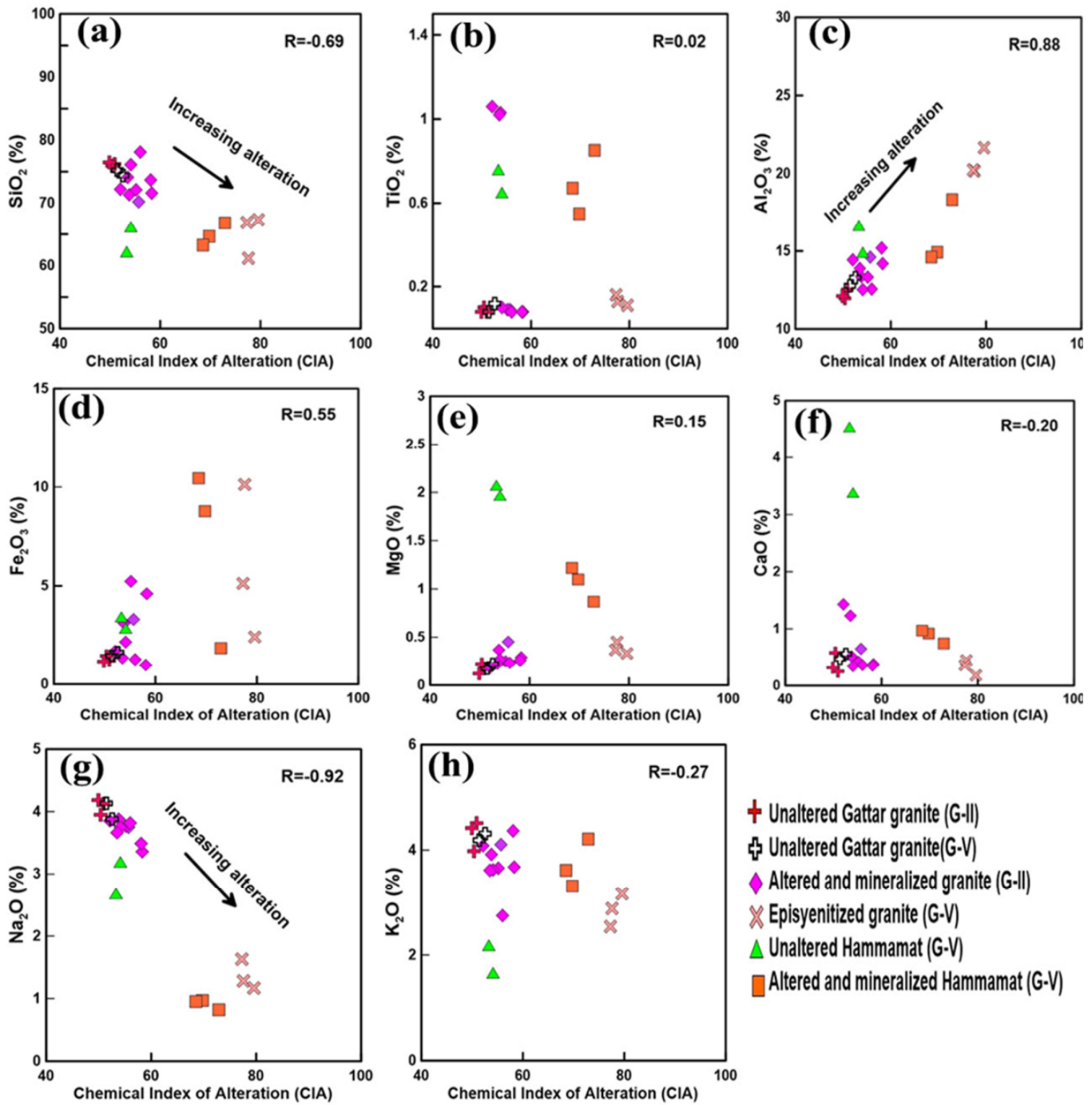


Figure 8. Major oxides (%) as a function of chemical index of alteration (CIA) for the studied rock samples from Gabal Gattar area.

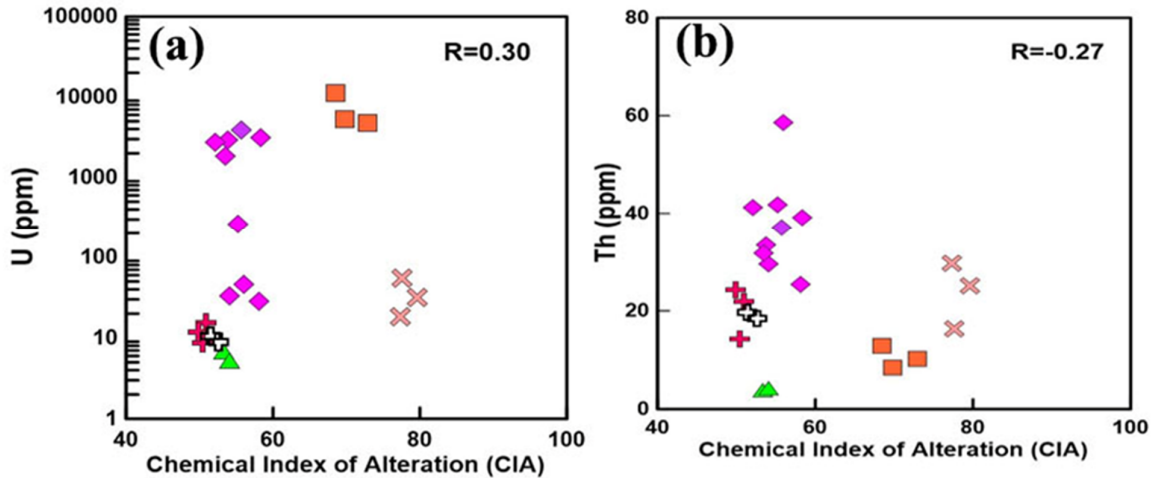


Figure 9. Variation of U and Th with the degree of alteration (CIA) for the studied rock materials in Gabal Gattar area. Symbols as in Figure 8.

4.4. Mechanical properties

The test results of the mechanical properties of the studied rock varieties are summarized in Table (4). Decreases in mechanical properties due to alteration and mineralization are illustrated in Figure (11). Unaltered Gattar granite shows a significantly elevated UCS values (av. 153MPa; G-II occurrence), higher than the standard specification limit (av. 131 MPa) of granite (ASTM C615/C15M) [36]. The altered and mineralized Gattar granite from G-II occurrence shows wide range (48-174MPa) according to the dominant type of alteration (Figure 10a). The silicified samples display elevated UCS (GII-S8 and GII-S9), whereas the kaolinitized sample (GII-K12) has the lowest UCS value. The degree of alteration increases towards the episyenitized samples and the UCS registered extremely lower values (av. 8 MPa). The unaltered Hammamat sediments have average of 112.5 MPa (Table 4) lower than the Gattar granite and extremely higher than the standard specification limit of sandstone 28MPa (ASTM C616/616M) [37]. Contrastingly, the altered mineralized Hammamat sediments show low UCS ranging from 34 to 64MPa, especially the bleached mineralized samples (GV-BM3 and GV-BM4). Generally, the UCS values are decreased with increasing the degree of alteration (CIA) values (Figure 11a) and mainly due to the formation of clay minerals that affect the strength properties of the altered rock. The investigated samples are classified according to the International Association for Engineering Geology and the Environment [38]. The unaltered granitic samples varied between strong and

extremely strong, the altered mineralized granitic samples range from strong to very strong, the unaltered Hammamat samples are strong, the altered mineralized Hammamat samples vary between moderately strong to strong and the episyenitized granitic samples are weak.

The unaltered Gattar granite yield average LAA of 25.78 % for G-II and 28.03% for G-V nearly matching with the standard specification limit (av. 25%) of granite (ASTM C615/C15M; Figure 10b) [36]. The unaltered Hammamat sediments give average LAA of 35.83%. The values of LAA % are increased with the degree of alteration (CIA) and a strong positive correlation ($r=0.95$) is calculated between the two variables (Figure 11b). The unaltered Hammamat sediments have average LAA (35.17%) higher than that of the mineralized granitic samples (av.=31.12%). The Hammamat samples were foliated and show their tendency of breakage along the foliation. The altered mineralized Hammamat and the episyenitized samples have the highest LAA averages of 52.57%, and 84.35%, respectively.

The SDI of the unaltered Gattar granite shows the highest values (av.= 98.4% for G-II samples and 97.46% for G-V samples (Table 4 and Figure 10c) nearly matching with the average value of fine-grained granite after two cycles with distilled water (99.085%) [39]. The unaltered Gattar granite is classified as high to very high durability according to Gambles' Slake Durability classification [40]. The unaltered Hammamat samples show also high durability and have average index value of 96.85%. The SDI values are decreased toward the altered varieties. Figure (11c) shows slake durability index values

plotted against degree of weathering (CIA) for samples from different rock exposures in Gattar area. Samples with the higher degrees of alteration show a wider range of durability when compared to their least altered equivalents. The altered and mineralized granite was classified with high durability (av. 96.57%), the altered mineralized Hammamat samples show medium durability (av. 84.45%), and the episyenitized samples were classified also with medium durability.

The altered mineralized Hammamat and episyenitized granitic samples have the highest CI averages of 93.83% and 94.88% respectively, compared to their unaltered equivalents of Hammamat sediments (av. 85.38%) and Gabal Gattar granite (av.77.13%). The average

crushability index of Gabal Gattar granite matches with the average crushability index 79.9 % (Figure 10d) for Rosa Porrino granite [41]. The CI values are positively correlated with the degree of alteration CIA ($r=0.82$) as shown in Figure (11d).

Range and average of the ISI of the studied samples are graphically represented in Figure (10e). The unaltered Gattar granite samples have averages ISI values of 63.21% (G-II) and 61.13% (G-V), lower than the average of ISI of 70.9 % for Rosa Porrino granite [41]. These data are decreased in the altered granite (av. 60.02%) and mineralized Hammamat samples (av. 60.02%), and the extremely lower values are recorded in the episyenitized granite (av. 30.79%). Generally, the impact strength values are negatively correlated with the degree of alteration CIA (Figure 11e).

Table 4. Results of mechanical properties of the studied rock varieties from Gattar area.

Location	Rock variety	Sample No.	Mechanical properties					Chemical Index of Alteration (CIA)	
			Compressive strength		Abrasion value (%)	Slake Durability index (%) after 2cycles	Crushability Index (%)		Impact Strength Index (%)
			MPa	Kg/cm ²					
G-II uranium occurrence	Unaltered Gattar granite	GII-FG1	142	1500	25.89	98.29	77.89	62.88	50.9
		GII-FG2	157	1571	25.81	98.34	77.35	63.21	50.4
		GII-FG3	160	1600	25.63	98.56	76.14	63.54	49.9
	Altered and mineralized Gattar granite	GII-M4	111	1110	32.17	96.15	77.71	61.72	55.7
		GII-M5	113	1130	31.37	97.08	76.74	58.76	53.8
		GII-M6	95	980	33.14	95.38	87.34	56.52	58.3
		GII-He7	121	1250	31.71	96.37	90.48	57.61	55.2
		GII-S8	169	1700	26.94	97.43	73.71	67.61	56
		GII-S9	174	1900	24.37	97.51	71.54	68.78	54.1
		GII-FL10	117	1170	29.64	97.14	74.13	61.71	53.5
		GII-FL11	120	1200	29.34	97.38	73.91	65.84	52.1
		GII-K12	48	500	41.38	94.67	91.49	41.62	58.1
G-V uranium occurrence	Unaltered Hammamat sediments	GV-HFr1	115	1148	35.17	97.18	84.92	52.56	53.3
		GV-HFr2	110	1100	36.49	96.51	85.83	51.45	54.1
	Altered and mineralized Hammamat sediments	GV-BM3	48	480	55.76	83.29	92.26	40.74	72.9
		GV-BM4	34	340	58.91	82.94	93.83	39.18	73.3
		GV-HM5	50	500	47.92	85.71	88.71	45.41	69.8
		GV-HM6	64	650	47.68	85.84	87.63	45.83	68.5
	Unaltered Gattar granite	GV-FG7	119	1200	28.41	97.37	79.74	61.11	52.6
		GV-FG8	130	1338	27.64	97.54	78.76	61.14	51.4
	Episyenitized Gattar granite	GV-Ep9	8	80	84.72	62.37	94.87	31.29	77.6
		GV-Ep10	4	40	85.34	60.67	95.41	28.14	79.6
		GV-Ep11	12	120	82.98	62.45	94.37	32.95	77.3

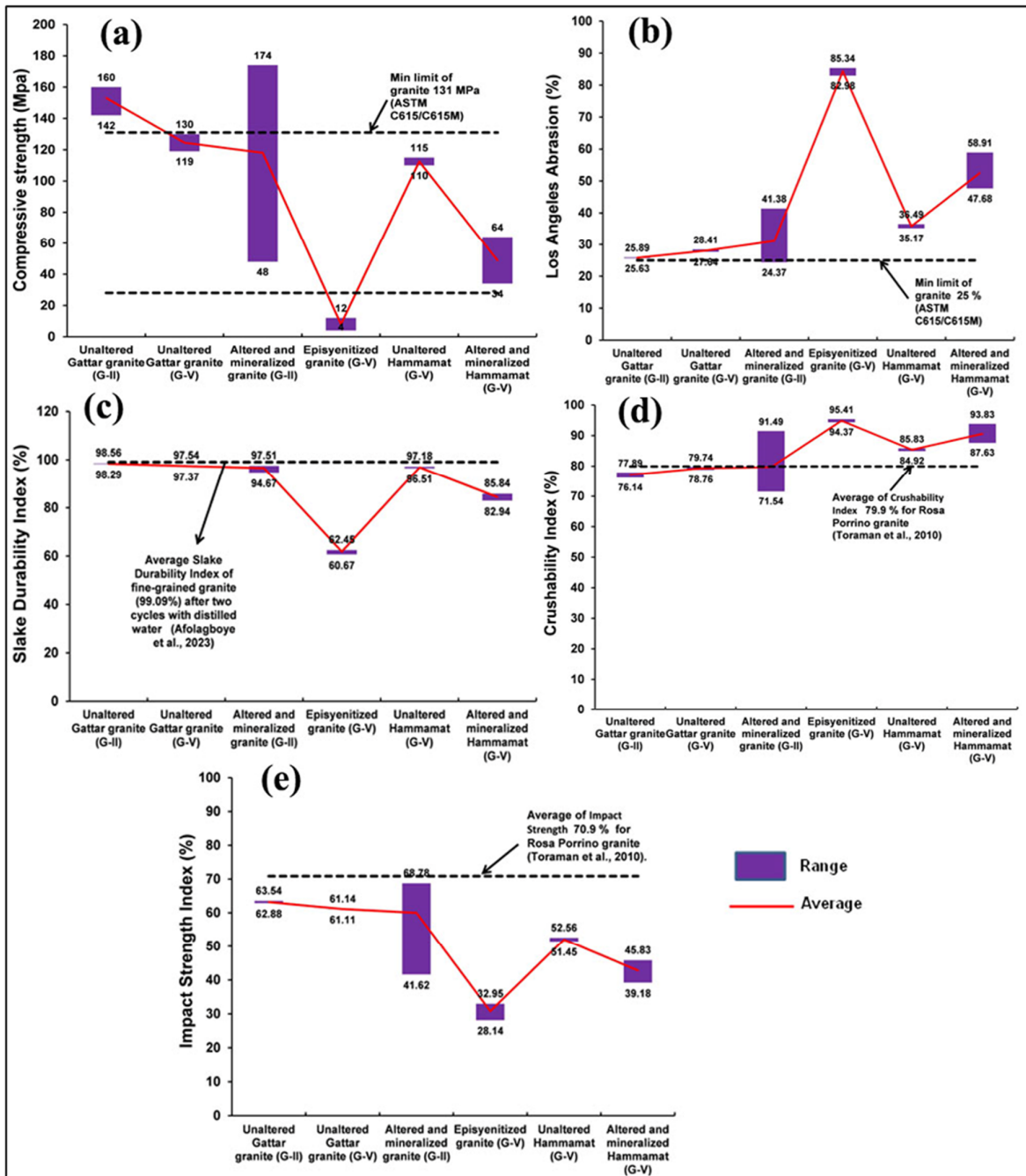


Figure 10. Ranges and averages of the mechanical tests for different rock facies in Gattar area. (a) Uniaxial compressive strength (MPa). (b) Los Angeles Abrasion (%). (c) Slake durability index (%). (d) Crushability index (%). (e) Impact strength index (%).

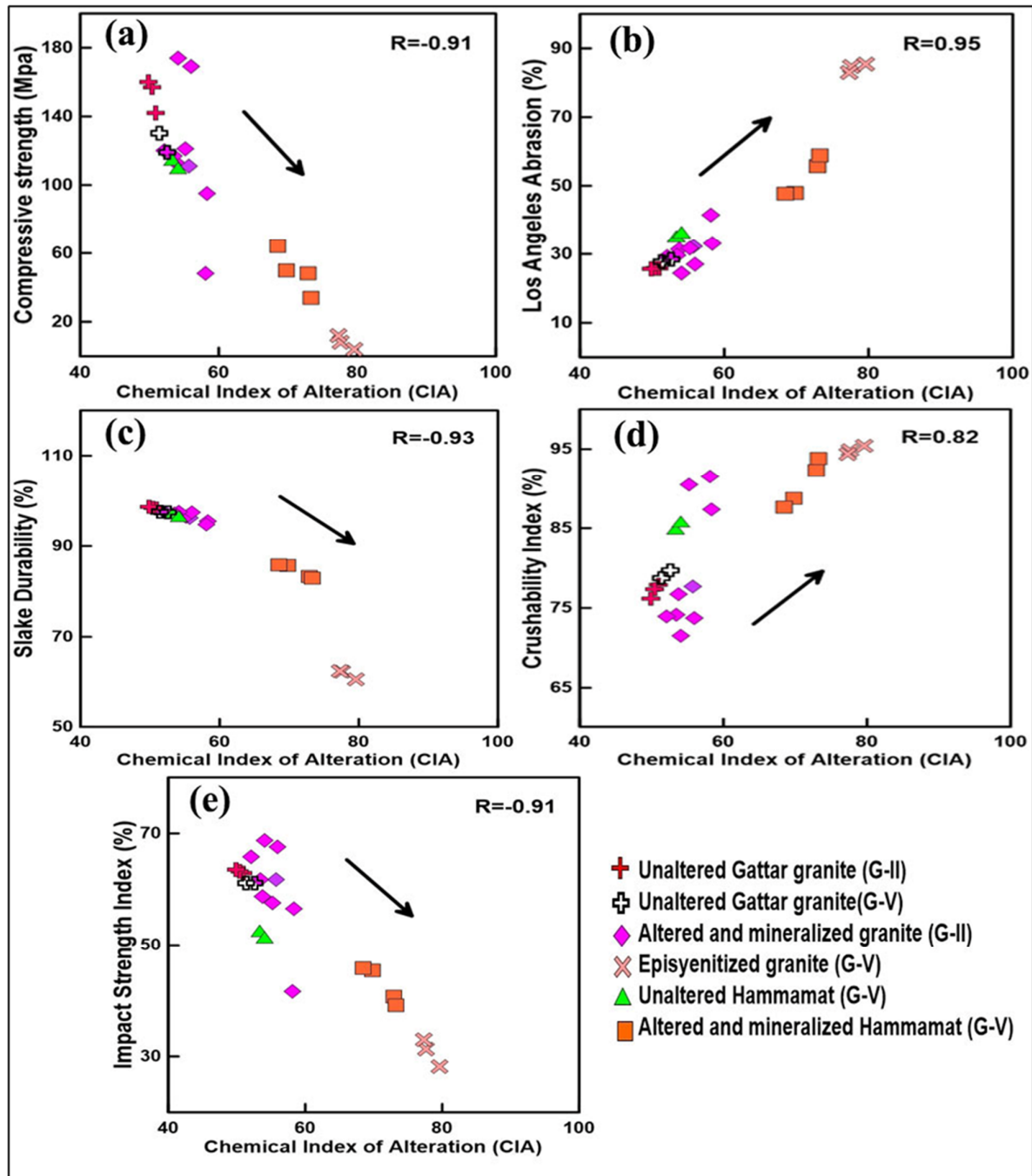


Figure 11. Relation between Chemical Index of Alteration (CIA) and the mechanical properties of the investigated rock varieties from Gabal Gattar area. (a) Uniaxial compressive strength (MPa). (b) Los Angeles Abrasion (%). (c) Slake durability index (%). (d) Crushability index (%). (e) Impact strength index (%).

4.5. Classification of alteration grades

The uranium-bearing rocks from Gattar area were subjected to the effects of late-magmatic hydrothermal alteration and also more recent surficial weathering. It should be emphasized that the alteration effects are progressive and variations in material grades can occur laterally as well as vertically in any rock mass. The material

alteration grades (classes) used in this work were established based on the calculated degree of alteration (CIA) and the mechanical properties of the individual sample and with the aid of the previous studies published on the weathering classification of granite given by [42, 43]. However, the term “Altered” was used to describe rock masses which have been affected by hydrothermal alteration. Table (5) presents the

alteration grades (AG) suggested in this work for the examined rocks from Gabal Gattara area. The rocks were divided into five categories: fresh (AG-I), slightly altered (AG-II), moderately altered (AG-III), highly altered (AG-IV) and very highly altered (AG-V). Moreover, the strength properties of the classified grades are illustrated in

Table (5). The common alteration grades varied from AG-1 to AG-V in the majority of sampling locations. However, in one location (G-II occurrence), it varied from AG-I to AG-III. Additionally, a change from fresh rock to highly altered rock is observed in G-V occurrence.

Table 5. Classification of alteration grades of the investigated rocks in terms of degree of alteration (CIA) and mechanical properties of the rock material.

Rock type	Sample	Descriptive term	Alteration GRADE (AG)	Degree of Alteration	Relative Strength	Durability
Unaltered perthitic granite	GII-FG1	Fresh	AG-I	49.9-52.6	Extremely strong to strong	Very High to High
	GII-FG2					
	GII-FG3					
	GV-FG7					
	GV-FG8					
Altered and mineralized perthitic granite	GII-M5	Slightly Altered	AG-II	52.1- 54.1	Very strong to strong	High
	GII-S9					
	GII-F10					
	GII-F11					
	GII-M4					
Episyenitized granite	GII-M6	Moderately Altered	AG-III	55.2- 58.3	Very strong to moderately Strong	High to Medium
	GII-He7					
	GII-S8					
	GII-K12					
	GV-Ep9					
GV-Ep10						
GV-Ep11						
Unaltered Hammamat sediments	GV-HFr1	Fresh	AG-I	53.3- 54.1	Strong	High
	GV-HFr2					
Altered and mineralized Hammamat sediments	GV-BM3	Highly Altered	AG-IV	68.5- 73.3	Strong to Moderately strong	Medium High to Medium
	GV-BM4					
	GV-HM5					
	GV-HM6					

In the Fresh granite, all the mineral constituents are hard and sound. It is generally extremely strong but the samples from G-V are more affected by surficial weathering and being strong. The fresh granite in the study area has CIA values ranging from 49.9 to 52.6. The durability of this granite is very high to high (Table 5). In the slightly altered Granite, a series of microcracks parallel to major joint surfaces are present in the stained zone. At more advanced stages of alteration, these microcracks develop in a radial arrangement surrounding the less altered variety. The strength of this grade varied between very strong and strong whereas the CIA values ranging from 52.1 to 54.1. The durability of this grade is high (Table 5). Moderately altered granite is brecciated and dominantly fractured; the microfractures filled by alteration minerals. The intact rock strength is appreciably reduced in the more altered specimens in this grade, in comparison to the fresh and slightly altered granite. The CIA values of this altered domain

ranges from 55.2 to 58.3. The relative strength of this grade is very strong to moderately strong and the durability is high to medium (Table 5). Very highly altered episyenitized granite can be a weak rock. It can be easily broken by the hand hammer. It is completely discolored, reddish brown to whitish light pink. The CIA values of this altered rock ranges from 77.3- 79.6 and its durability is medium (Table 5).

The fresh samples of the Hammamat sediments are commonly foliated and its relative strength is strong. The CIA values (53.3- 54.1) are slightly higher than those of the Fresh granite and the durability is strong (Table 5). In the altered and mineralized Hammamat, the presence of excessive alterations in the fault and fracture zones make relative strength of this grade varied between strong to moderately strong. The CIA values of this grade range from 68.5- 73.3 and the durability is medium high to medium (Table 5).

The characterization of the rocks is helpful to describe drilling penetration resistance and to

illustrate feasibility for ore processing as well as preparing the designs of tunnels. In many locations in the Eastern Desert of Egypt the main host rock for the uranium mineralization is the granite that was subjected to the same hydrothermal processes affected in Gabal Gattar area. However, in these uranium occurrences, the Nuclear Materials Authority of Egypt carried out intensive program for uranium ore extraction and processing. So, this classification scheme of alteration grades can be used as a supplement to the general mass weathering scheme adopted for the grouping and subdivision of the weathered granite for engineering purposes.

5. Conclusions

The present work describes the relative changes occurring in the rock material caused by hydrothermal alteration with respect to their unaltered equivalent (fresh) and introduces a classification scheme for alteration grades of the investigated rock types in Gattar area, Northern Eastern Desert, Egypt. The degree of alteration of the hydrothermally uranium-mineralized rocks in the most significant uranium occurrences (G-II and G-V) is evaluated by the calculation of chemical index of alteration (CIA). The mechanical properties of the studied samples were evaluated using the following tests: uniaxial compressive strength, slake durability index, Los Angeles abrasion, crushability index and impact strength index. Five rock varieties were discriminated in the studied occurrences, which represent the unaltered and altered uranium-mineralized rocks including: (1) unaltered Gattar granite, (2) altered and mineralized Gattar granite, (3) unaltered Hammamat, (4) altered and mineralized Hammamat (bleached and hematized varieties), and (5) episyenitized Gattar granite. Differences in the rock chemistry (change in major oxide values) in the transition from fresh rock to moderately altered rock, from moderately altered to highly altered rock, indicate variance impacts of the hydrothermal alteration and weathering events, and this development of alteration grades is also revealed in the calculations of chemical index of alteration (CIA). The studied rocks were classified into five grades: fresh (AG-I), slightly altered (AG-II), moderately altered (AG-III), highly altered (AG-IV) and very highly altered (AG-V). The strength properties of the investigated rock units corresponded well with the alteration grades assigned to them. The fresh Gattar granite is generally extremely strong and

its durability is very high to high. The altered mineralized granite from G-II is very strong to strong with durability varying between high to medium. The episyenitized granite is a weak rock with medium durability. The fresh Hammamat is a strong rock with high durability and the altered mineralized Hammamat is strong to moderately strong with medium durability. The classification scheme suggested in this work is useful for the engineering purposes in Gabal Gattar area which can reduce the cost of tunneling, drilling, crushing and grinding processes.

Acknowledgements

The authors would like to thank Prof. Dr. Amr A. Abdel Hamid, Professor of Geology in the Nuclear Materials Authority, for their comments and suggestions, which greatly improved the manuscript. Grateful thanks are given to all staffs in Nuclear Materials Authority and Mining Engineering Dep., Al Azhar Univ., for their kind cooperation, various forms of assistance and fruitful discussions.

References

- [1]. El-Bialy, M. Z., & Omar, M. M. (2015). Spatial association of Neoproterozoic continental arc I-type and post-collision A-type granitoids in the Arabian–Nubian Shield: The Wadi Al-Baroud Older and Younger Granites, North Eastern Desert, Egypt. *Journal of African Earth Sciences*, 103, 1–29.
- [2]. Roz, M. E. (1994). Geology and uranium mineralization of Gabal Gattar area, North Eastern Desert, Egypt. *M.Sc. Thesis, Faculty of science, Al Azhar University*.
- [3]. Abdel Hamid, A. A. (2006). Geologic factors controlling the radon emanation associated with uranium mineralization along Wadi Belih, NED, Egypt. *Unpublished M.Sc. Thesis, Faculty of science, Benha University*.
- [4]. Mahdy, N. M., El Kalioubi, B. A., Wohlgemuth - Ueberwasser, C. C., Shalaby, M. H., & El Afandy, A. H. (2015). Petrogenesis of U- and Mo-bearing A₂-type granite of the Gattar batholith in the Arabian Nubian Shield, Northeastern Desert, Egypt: Evidence for the favorability of host rocks for the origin of associated ore deposits. *Ore Geology Reviews*, 71, 57–81.
- [5]. El Sundoly, H. I., & Waheeb, A. G. (2015). A new genetic model for the localization of uranium minerals at the northern part of Gabal Gattar, North Eastern Desert, Egypt. *Third Symposium of the Geological Resource in the Tethys Realm, Cairo University*.
- [6]. El Kholy, D.M., Khamis, H.A., El Sundoly., & H.L. (2019). Geology and structural relationship

between uranium occurrences in the northern part of Gabal Gattar, Northern Eastern Desert, Egypt. *Nuclear Sciences Scientific Journal*, 8A, 1–18.

[7]. Abdel Hamid, A.A., Abdel Hamid, H. M., Seddik, H.S., & Metwally, M. (2023). Mineralization styles and alteration paragenesis of metasomatic zones in the highly fractionated granite of Gabal Gattar, Northern Eastern Desert, Egypt. *Middle East Journal of Applied Sciences*, 13, 441-457.

[8]. Raslan, M.F. (2009). Occurrence of uraniferous iron grains at Gabal Gattar, El Missikat and El Erediya granites in Eastern Desert of Egypt. *Resource Geology*, 59, 99-105.

[9]. Mahdy, N.M., Shalaby, M. H., Helmy, H. M., Osman, A.F., El Sawey, E. H., & Abu Zeid, E. K. (2014). Trace and REE element geochemistry of fluorite and its relation to uranium mineralizations, Gabal Gattar Area, Northern Eastern Desert, Egypt. *Arabian Journal of Geoscience*, 7, 2573–2589

[10]. El Terb, R. A., Nigm, A. A., Hosny, A. A., & Elawadi, A. E. (2006). Geophysical study of the contact Zone between the granitic rocks and Hammamat sediments in G-V Prospect, Gabal Gattar, Northeastern Desert, Egypt. Conference: Intern. Conf. Geol. *The Arab World (GAW)*, 8, 215-222.

[11]. El Zalaky, M. A. (2007). Geology and remote sensing studies on some uranium-bearing granites, Eastern Desert, Egypt. *Unpublished Ph.D. Thesis, Faculty of Science, Benha University*.

[12]. El Kholy, D. M., El Husseiny, M. O., Saleh, W. H., El Zalaky., & M. A. (2012). Remote sensing, geology and geochemistry on the GVIII uranium mineralization, Gabal Gattar, North Eastern Desert, Egypt. *Nuclear Sciences Scientific Journal*, 1, 69- 84

[13]. Haridy, M. H. (1995). Physical and mechanical properties of Gabal Gattar granitic pluton and the relation to joint-type U-mineralization. *M.Sc. Thesis, Faculty of Science, Cairo University*.

[14]. Salah El Din, M. (2017). Effects of Geotechnical properties of some granitic rocks in underground mining in the African Nubian Shield. *M. Sc. Thesis, Department of Natural Resources, Cairo University*.

[15]. Voicu, G., & Bardoux, M. (2002). Geochemical behavior under tropical weathering of the Barama–Mazaruni greenstone belt at Omai gold mine, Guiana shield. *Appl. Geochemistry*, 17, 321 – 336.

[16]. Babechuk, M.G., Widdowson, M., & Kamber, B.S. (2014). Quantifying chemical weathering intensity and trace element release from two contrasting basalt profiles, Deccan Traps, India. *Chemical Geology*, 363, 56–75.

[17]. Mangold, N., Dehouck, E., Fedo, C., Forni, O., Achilles, C., Bristow, T., Downs, R.T., Frydenvang, J., Gasnault, O., L'Haridon, J., Le Deit, L., Maurice, S., McLennan, S.M., Meslin, P.-Y.,

Morrison, S., Newsom, H.E., Rampe, E., Rapin, W., Rivera-Hernandez, F., Salvatore, M., & Wiens, R.C. (2019). Chemical alteration of fine-grained sedimentary rocks at Gale crater. *Icarus*, 321, 619–6.

[18]. Duzgoren-Aydin, N., Aydin, A., & Malpas, J. (2002). Distribution of clay minerals along a weathered pyroclastic profile, Hong Kong. *Catena*, 50, 17 – 41.

[19]. Meunier, A., Caner, L., Hubert, F., El Albani, A., & Pret, D. (2013). The weathering intensity scale (WIS): an alternative approach of the chemical index of alteration (CIA). *American Journal of Science*, 313, 113–143.

[20]. Bozkurtoglu, E., Karakas, A., & Özdamar, S. (2022). Evaluation of weathering and alteration effects by rock change value (RCV) and weathering indices of volcanic rocks in the Şile Region (NW Turkey). *Arabian journal of Geoscience*, 15, 1543.

[21]. Jaques, D.S., Marques, E.A., Marcellino, L.C., Leão, M.F., & Coelho, V.S. (2021). Morphological and mineralogical characterization of weathering zones in tropical climates: A basis for understanding the weathering process on granitic rocks in southeastern Brazil. *Journal of South American Earth Sciences*, 108, 103187.

[22]. Moussa, E. M., Stern, R. J., Manton, W. J., & Ali, K. A. (2008). SHRIMP zircon dating and Sm/Nd isotopic investigations of Neoproterozoic granitoids, Eastern Desert, Egypt. *Precambrian Research*, 160, 341-356.

[23]. El Sayed, M. M., Shalaby, M. H., & Hassanen, M. A. (2003). Petrological and geochemical constraints on the tectonomagmatic evolution of the late Neoproterozoic granitoid suites in the Gattar area, North Eastern Desert, Egypt. *Neues Jahrbuch für Mineralogie Abhandlungen*, 178, 239-275.

[24]. Mouhareb, R. Sh. (2017). Petrographical and mineralogical studies of Hammamat sediments and Gattarian granite along Wadi Belih, north Eastern Desert, Egypt. *Journal of Petroleum and Mining Engineering*, 19, 63-70.

[25]. ASTM E-1621. (2013). Standard guide for elemental analysis by wavelength dispersive x-ray fluorescence spectrometry. *American society for testing and materials, West Conshohocken, PA, USA*.

[26]. Shapiro, L., & Brannock, W. W. (1962). Rapid analysis of silicate, carbonate and phosphate rocks. *U. S. Geol. Surv. Bull*, 4A, 111.

[27]. Marczenko, Z. (1986). Spectrophotometric determination of elements. *New York: John Wiley and Sons*.

[28]. ISRM. (1981). Rock Characterization, Testing and Monitoring, ISRM Suggested Methods, edited by E. T. Brown, Pergamon Press, Oxford.

- [29]. ASTM C131/131M. (2014). Resistance to degradation of small-size coarse aggregate by abrasion and impact in the Los Angeles Machine, *American society for testing and materials, West Conshohocken, PA, USA*.
- [30]. ASTM D4644_08. (2008). Standard method for slake durability of shales and similar weak rocks. *ASTM International, West Conshohocken, PA, USA*.
- [31]. Evans, I., & Pomeroy, C.D. (1966). The strength, fracture and workability of Coal. *Pergamon Press, London*.
- [32]. Nesbitt, H.W., & Young, G.M. (1982). Early Proterozoic climates and plate motions inferred from major element chemistry of lutites. *Nature*, 299, 715-717.
- [33]. Haskins, D. (2006). Chemical and mineralogical weathering indices as applied to a granite saprolite in South Africa. *The Geological Society of London*, 465. IAEG.
- [34]. Rogers, J. J. W., & Adams, J. A. S. (1969). Thorium-Uranium. In: K. H. Wedepohl (Ed.), *Handbook of Geochemistry. Berlin, Springer-verlag, Vol. 2, No. 3, Chap.90&92*.
- [35]. Killen, P. G. (1979). Gamma ray spectrometric methods in uranium exploration – application and interpretation. In: P. J. Hood (Ed.), *Geophysics and Geochemistry in the search for Metallic Ores. Geological Survey of Canada, Economic Geology*, 31, 163-229.
- [36]. ASTM C615/C615M. (2011). Standard specification for granite dimension stone, *American society for testing and materials, West Conshohocken, PA, USA*.
- [37]. ASTM C616/C616M. (2015). Standard specification for quartz-based dimension stone, *American society for testing and materials, West Conshohocken, PA, USA*.
- [38]. IAEG. (1979). Classification of rocks and soils for engineering geological mapping part I: Rock and soil materials. *Bull. International Association of Engineering Geology*, 19, 364 – 371.
- [39]. Afolagboye, L.O., Owoyemi, O.O., & Akinola, O.O. (2023). Effect of pH condition and different solution on the slake durability of granitic rocks. *Geotechnical Geological Engineer*, 41, 897–906.
- [40]. Goodman, R.E. (1989). Introduction to Rock Mechanics. 2nd Edition, *John Wiley & Sons Ltd., New York*.
- [41]. Toraman, O.Y., Kahraman, S., & Cayirli, S. (2010). Predicting the crushability of rocks from the impact strength index. *Minerals Engineering*, 23, 752-754.
- [42]. Irfan, T. Y., & Dearman, W. R. (1978). Engineering classification and index properties of a weathered granite, *Bull. International Association of Engineering Geology*, 17, 79-90.
- [43]. GCO. (1988). Guide to Rock and Soil Descriptions (Geoguide 3). *Geotechnical Control Office, Hong Kong*.

شاخص شیمیایی دگرسانی و ارتباط آن با خواص مکانیکی سنگ های معدنی اورانیوم هیدروترمال در منطقه گبال گتار، صحرای شمال شرقی، مصر

یحیی ز. درویش^۱، عبدالرحیم امبابی^{۲*}، سمیر ام. سلیم^۲، درویش م. الخولی^۱، هانی ای. شرف‌الدین^۲، و حسین ع. فرگ^۲

۱- سازمان مواد هسته ای مصر، P.O. جعبه ۵۳۰، المادی، قاهره، مصر

۲- گروه مهندسی معدن و نفت، دانشکده فنی، دانشگاه الازهر، قاهره، مصر. ارسال ۲۱/۰۱/۲۰۲۴، پذیرش ۰۱/۰۶/۲۰۲۴

* نویسنده مسئول مکاتبات: Abdel-raheemkhalifa.12@azhar.edu.eg

چکیده:

گرانیت‌های جوان تر منطقه گبال گتار، صحرای شمال شرقی مصر، میزبان کانی‌سازی اورانیوم گرمایی در بخش شمالی باتولیت گتار و در امتداد تماس آن با قدیمی‌ترین رسوبات حمامات هستند. سنگ‌های میزبان بسیاری از ویژگی‌های نتایج رونوشت هیدروترمال را در تغییر ویژگی‌های مهندسی اولیه خود به عنوان تابعی از تغییرات درجه دگرسانی نشان می‌دهند. پیشرفت از کمتر تغییر یافته به سنگ های تغییر یافته و کانی شده به عنوان نتیجه فرآیندهای دگرسانی توسط شاخص شیمیایی دگرسانی (CIA) ارزیابی شد. مقادیر عددی CIA با نسبت مولکولی Al به کاتیون‌های کلسیم، سدیم و پتاسیم محاسبه شد. سنگ‌های مورد مطالعه بر اساس درجه دگرسانی و ویژگی‌های مقاومتی به پنج درجه تقسیم شدند: تازه (AG-I)، کمی دگرسان شده (AG-II)، تغییرات متوسط (AG-III)، بسیار تغییر یافته (AG-IV) و بسیار زیاد (AG-V) تغییر یافته است. خواص مقاومتی واحدهای سنگی مورد مطالعه به خوبی با درجه دگرسانی اختصاص داده شده به آنها همبستگی دارد. به این معنا که با افزایش درجه از AG-I به AG-V، مقاومت سایشی و شاخص خردشدگی افزایش یافت، در حالی که مقاومت فشاری، دوام لغزش و مقاومت ضربه کاهش یافت.

کلمات کلیدی: شاخص شیمیایی دگرسانی، خواص مکانیکی، دگرسانی هیدروترمال، کانی سازی اورانیوم، منطقه گتار.